Injection locking of an electronic maser in the hard excitation mode

K. A. Yakunina,[1] A. P. Kuznetsov,[1,2] and N. M. Ryskin[1,2]
[1]Saratov State University, 83 Astrakhanskaya St., 410012 Saratov, Russia
[2]Department of Nonlinear Physics, Saratov Branch, V.A. Kotel'nikov Institute of Radio Engineering and Electronics, 38 Zelenaya St., 410019 Saratov, Russia

(Received 1 July 2015; accepted 2 November 2015; published online 18 November 2015)

The phenomenon of hard excitation is natural for many electronic oscillators. In particular, in a gyrotron, a maximal efficiency is often attained in the hard excitation regime. In this paper, we study the injection-locking phenomena using two models of an electronic maser in the hard excitation mode. First, bifurcation analysis is performed for the quasilinear model described by ordinary differential equations for the slow amplitude and phase. Two main scenarios of transition to the injection-locked mode are described, which are generalizations of the well-known phase-locking and suppression mechanisms. The results obtained for the quasilinear model are confirmed by numerical simulations of a gyrotron with fixed Gaussian structure of the RF field. © *2015 AIP Publishing LLC*.
[http://dx.doi.org/10.1063/1.4935847]

I. INTRODUCTION

In the theory of self-oscillating systems, usually one distinguishes two different kinds of self-excitation, namely, soft and hard excitation.[1–4] In the soft excitation mode, an unstable noise-level perturbation grows and evolves into a self-sustained oscillation. Conversely, in the hard excitation mode, a self-oscillation settles only for a sufficiently intensive initial perturbation with amplitude exceeding a certain threshold, while a small perturbation decays. The phenomenon of hard excitation is natural for many electronic oscillators. In particular, in a gyrotron, a maximal efficiency is often attained in the hard excitation regime.[5]

In recent years, the problem of injection locking of microwave electron oscillators has attracted significant interest. The injection locking is widely used to stabilize the radiation frequency and phase of high-power microwave sources[6–10] as well as to reduce transient times.[10,11] In addition, a low-power external driving of a high-power oscillator may result in the fast frequency step-tuning owing to the mode switching effect.[12–15] Control of radiation frequency is of primary importance for the electron-cyclotron plasma heating systems, where several gyrotrons are used that have to generate a signal at the same frequency.

Injection locking of an oscillator in the hard excitation mode has been studied in several works (see Ref. 2). However, the general pattern of synchronization is still poorly understood. This work is aimed at studying injection-locked operation of a resonant electronic maser in the hard excitation mode. The article is organized as follows. In Sec. II, we introduce a simplified quasilinear model of a single-mode oscillator with hard excitation driven by an external harmonic signal. The model is described by the equations for slowly varying amplitude and phase. In Sec. III, the bifurcation mechanisms leading to the establishment of a synchronous mode are studied analytically and numerically. In Sec. IV, results of time-domain numerical simulations for a gyrotron with the Gaussian fixed structure of the high-frequency field are presented. Finally, the results and conclusions are summarized in Sec. V.

II. QUASILINEAR MODEL OF A RESONANT ELECTRONIC MASER

The quasilinear theory has been widely used to describe mode interaction processes in gyrotrons,[5,16–18] as well as in many other resonant electron[19,20] and optical[21] masers. Following Refs. 5 and 16–21, consider the RF field as a cold cavity eigenmode with a slowly varying amplitude $A(t)$, which obeys the excitation equation[6]

$$\frac{dA}{dt}+\frac{\omega_0 A}{2Q}=\omega_0 I_s\Phi(A)A+\frac{\omega_0 f_{inj}}{Q}e^{i(\omega_{inj}-\omega_0)t}, \qquad (1)$$

where ω_0 is the eigenfrequency, Q is the Q-factor, I_s is the normalized beam current parameter, $\Phi=\Phi'+i\Phi''$ is the complex gain function, f_{inj} and ω_{inj} are driving amplitude and frequency, respectively. In the framework of the quasilinear theory,[5,16] Φ is expressed as a polynomial expansion on $|A|^2$,

$$\Phi\approx\alpha-\beta|A|^2-\gamma|A|^4+\cdots, \qquad (2)$$

where the complex coefficient $\alpha=\alpha'+i\alpha''$ characterizes linear gain, while $\beta=\beta'+i\beta''$ and $\gamma=\gamma'+i\gamma''$ characterize nonlinear effects of first and second order, respectively. The hard excitation occurs if $\beta'<0$, i.e., the first-order nonlinear effect leads to growth of the amplitude instead of saturation. In such a case, one should retain the $\gamma|A|^4$ term in Eq. (2) assuming that $\gamma'>0$.

After substituting Eq. (2) into Eq. (1) and introducing normalized variables

$$t_{norm}=\frac{\omega_0 I_s\gamma'}{|\beta'|^2}t,\quad A_{norm}=A\sqrt{\frac{\gamma'}{|\beta'|}}\exp\left[-i(\omega_{inj}-\omega_0)t\right],$$

we obtain (the subscript "norm" is omitted hereafter)

$$\frac{dA}{dt} + i\Omega A = \left(\sigma + (1+ib)|A|^2 - (1+ic)|A|^4\right)A + f. \quad (3)$$

In Eq. (3), $f = \frac{f_{inj}}{QI_s}\frac{\gamma'}{|\beta'|^2}$ and $\Omega = \frac{\gamma'\left(\omega_{inj} - \omega_0(1+I_s\alpha'')\right)}{\omega_0 I_s|\beta'|^2}$ are the normalized driving amplitude and frequency mismatch, respectively, $\sigma = (\alpha' - \frac{1}{2QI_s})\frac{\gamma'}{|\beta'|^2}$ is the mode increment, $b = \beta''/|\beta'|$, and $c = \gamma''/\gamma'$.

III. ANALYSIS AND SIMULATION OF THE QUASILINEAR MODEL

A. Fixed points and analysis of their stability

Let us rewrite Eq. (3) as a system of two ordinary differential equations (ODEs) for real amplitude and phase, $A = a\exp(i\varphi)$,

$$\frac{da}{dt} = (\sigma + a^2 - a^4)a + f\cos\varphi,$$
$$\frac{d\varphi}{dt} = -\Omega + ba^2 - \frac{f}{a}\sin\varphi. \quad (4)$$

Henceforth, we assume $c = 0$, which is reasonable in a typical case.[17]

Consider a fixed-point solution of Eq. (4), $a = a_0 = \text{const}$, $\varphi = \varphi_0 = \text{const}$. When $-1/4 < \sigma < 0$, the free-running oscillator ($f = 0$) has two non-trivial fixed-point solutions

$$a_0^{\pm} = \frac{1 \pm \sqrt{1+4\sigma}}{2}, \quad (5)$$

which correspond to the stable and unstable limit cycles, i.e., hard excitation is possible. In addition, there exists a zero solution $a_0 = 0$, which is stable at $\sigma < 0$.

When $f > 0$, a fixed-point solution of Eq. (4) corresponds to a phase-locked state of the oscillator. One can easily derive an equation, which determines the resonant curves, i.e., the amplitude of the locked oscillation as a function of the frequency Ω,

$$[(\sigma + M - M^2)^2 + (\Omega - bM)^2]M = f^2, \quad (6)$$

where $M = a_0^2$ is the normalized intensity.

To investigate the stability of the fixed points, consider a slightly perturbed solution $a = a_0 + \tilde{a}$, $\varphi = \varphi_0 + \tilde{\varphi}$, where the perturbations evolve as $\tilde{a}, \tilde{\varphi} \sim \exp(\lambda t)$. After substituting into Eq. (4) and linearization, we arrive at the characteristic equation

$$\lambda^2 + 2A\lambda + B = 0,$$

where

$$A = -(\sigma + 2M - 3M^2), \quad (7)$$

$$B = (\sigma + 2M - 3M^2)^2 + (\Omega - 2bM)^2 - ((1-2M)^2 + b^2)M^2. \quad (8)$$

The stability conditions of a fixed point read[1,3]

$$A > 0, B > 0.$$

Equations (6)–(8) allow plotting the resonance curves together with the stability bounds. Fig. 1(a) presents the example of the resonance curves for the isochronous oscillator ($b = 0$). Different branches of the resonance curves merge at the critical points

$$M_{1,2} = \frac{3 \pm \sqrt{9+20\sigma}}{10}, \quad (9)$$

$$\Omega = \beta M_{1,2}, \quad (10)$$

and at the critical values of the driving force

$$f_{1,2} = \sqrt{M_{1,2}}|\sigma + M_{1,2} - M_{1,2}^2|. \quad (11)$$

In Fig. 1(a), these points are shown with white circles.

The $A = 0$ condition defines two horizontal lines on the (Ω, M) plane

$$M = \frac{1}{3}\left(1 \pm \sqrt{1+3\sigma}\right), \quad (12)$$

which are the bounds of Andronov–Hopf (AH) bifurcation. The $B = 0$ condition defines two closed curves, which are the bounds of saddle-node (SN) bifurcation. Accordingly, there exist two different mechanisms of synchronization.

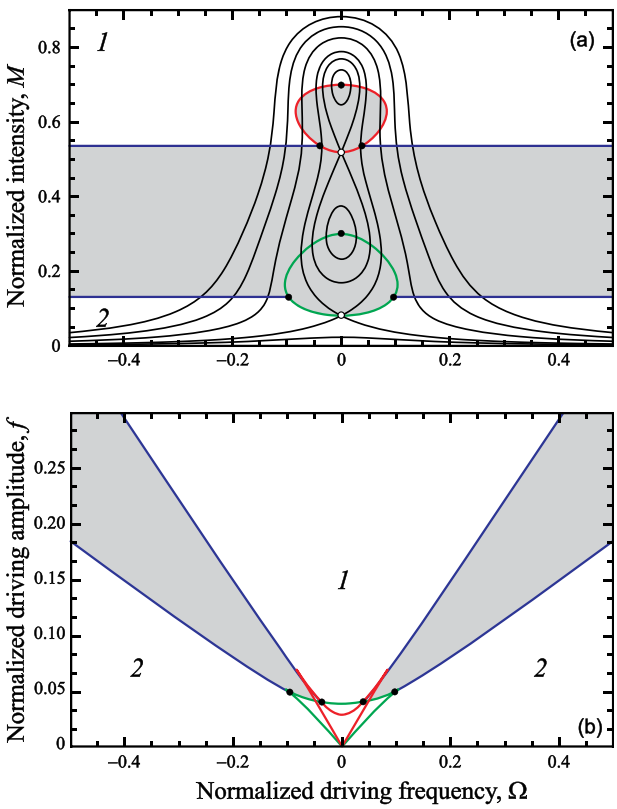

FIG. 1. Resonance curves (a) and synchronization tongues (b) for $\sigma = -0.21$, $b = 0$. "1" and "2" denote the domains of injection locking and regenerative amplification, respectively. The domain of beating is shaded.

The phase/frequency locking mechanism is associated with the SN bifurcation, while synchronization via suppression of the natural oscillation is associated with the AH one.[1–4]

In addition, using Eqs. (6)–(8), one can plot the stability bounds on the (Ω, f) plane presented in Fig. 1(b). On the contrary to the well-known pattern of synchronization for an oscillator with soft self-excitation,[1–5] these bounds have a form of two synchronization tongues, which correspond to injection locking of the stable (the inner tongue) and unstable (the outer tongue) limit cycle, respectively.

In the hard excitation mode, only a sufficiently large perturbation evolves into a stable periodic self-oscillation, while a perturbation with amplitude below certain threshold decays.[1–5] Thus, the driven oscillator may operate as a regenerative amplifier of a small input signal. In Fig. 1(a), only the states above the upper bound correspond to the phase-locked self-oscillation (domain *1*), while the states below the lower one (domain *2*) correspond to the regenerative amplification. The domain of unstable steady states is shaded. Note that in Fig. 1(b) at small Ω, two SN bounds partially overlap. In this domain, bistability is observed, i.e., both injection locking and amplification modes are stable. Between the upper and lower bounds of AH bifurcation, there are no stable fixed points. In this domain, only quasi-periodic oscillation with two independent frequencies exists. Such a regime is known as beating.

Figs. 2–4 illustrate transformation of the resonance curves and synchronization tongues with variation of the parameter of reactive nonlinearity b. Similar to the oscillator with soft excitation,[1–4] the resonance curves acquire

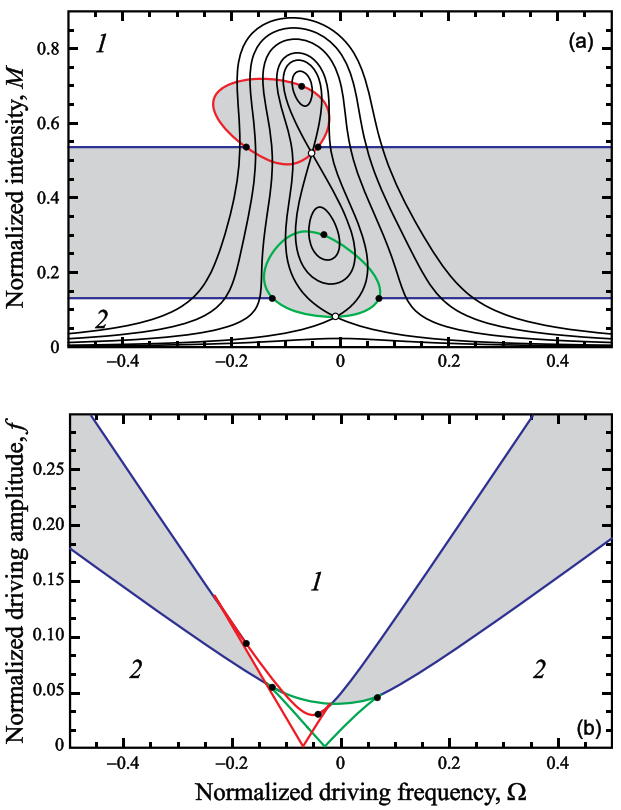

FIG. 2. Resonance curves (a) and synchronization tongues (b) for $\sigma = -0.21$, $b = -0.1$.

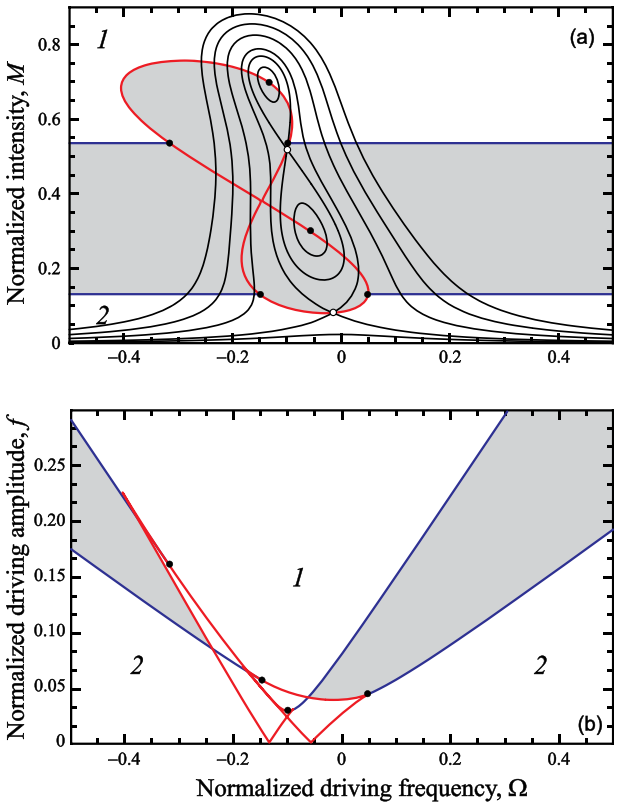

FIG. 3. Resonance curves (a) and synchronization tongues (b) for $\sigma = -0.21$, $b = -0.192$.

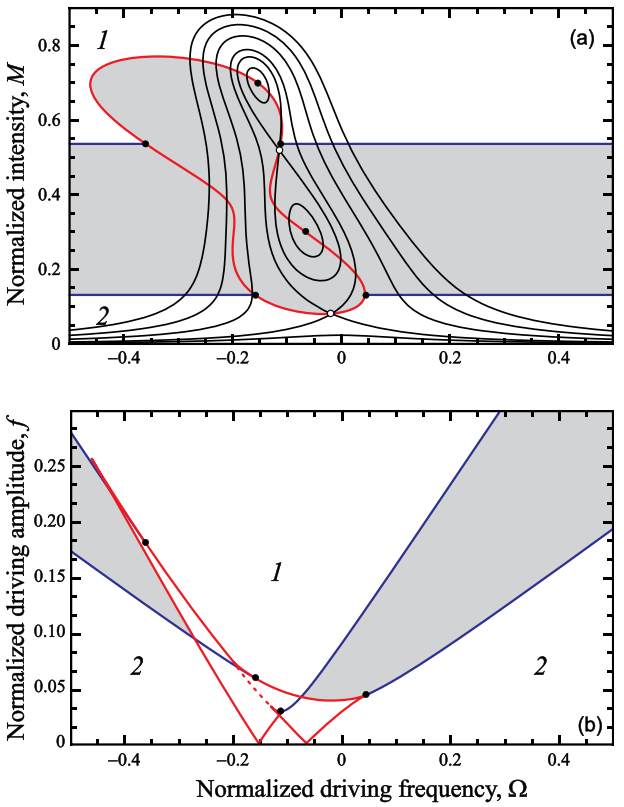

FIG. 4. Resonance curves (a) and synchronization tongues (b) for $\sigma = -0.21$, $b = -0.22$. The global bifurcation of the unstable cycle is shown by dots in Fig. 4(b).

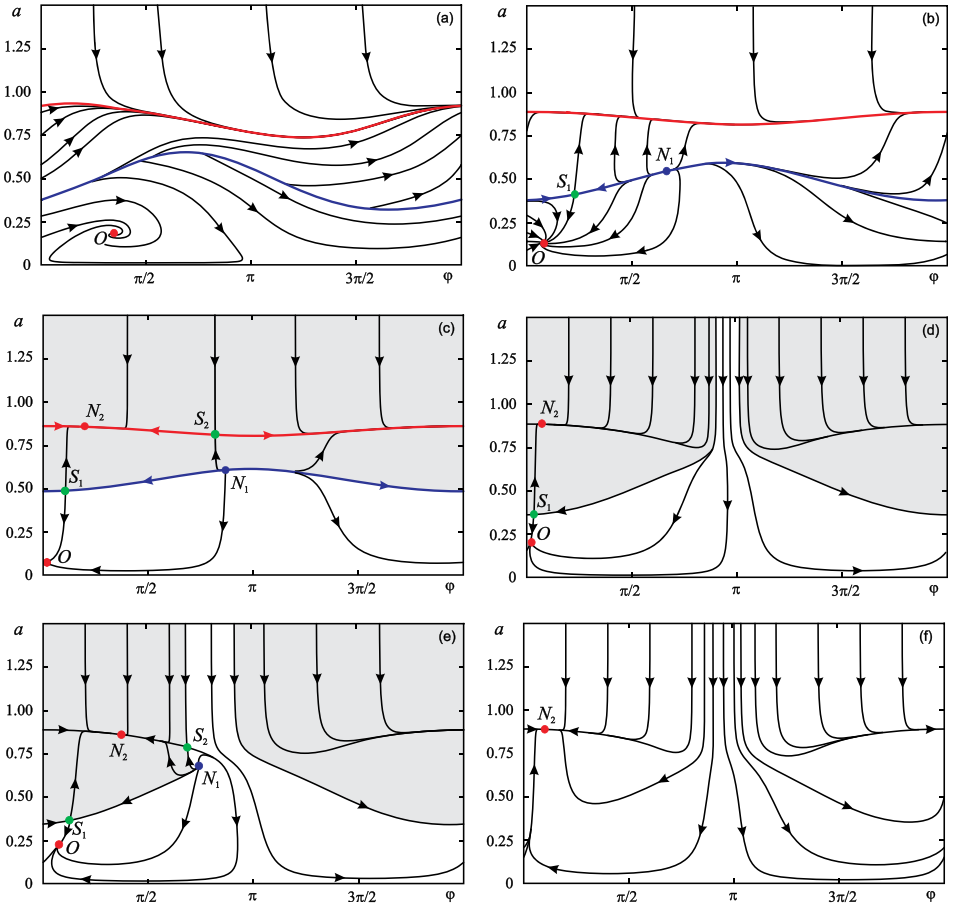

FIG. 5. Phase portraits illustrating transition to synchronization via the frequency locking scenario: $\sigma = -0.21$, $b = 0.0$, corresponding values of f and Ω are shown in Fig. 6. In (c)–(e), basins of attraction of the high-amplitude injection-locked state are shaded.

frequency shift $\Omega = bM$. The synchronization tongues touch the Ω axis in different points $\Omega_{1,2} = b(a_0^{\pm})^2$, where $a_0^{\pm}$ is given by Eq. (5).

Moreover, with the increase in b, two bounds of SN bifurcation merge into one, as shown in Figs. 3(a) and 4(a), and two distinct synchronization tongues merge accordingly [Figs. 3(b) and 4(b)]. The scenario of merging has been described in detail in Ref. 22, where injection locking of a general model of a self-oscillatory system with coexisting stable and unstable limit cycles has been studied.

B. Simulation of the injection locking scenarios

Direct numerical integration of Eq. (4) not only confirms the results of stability analysis presented in Sec. III A but also reveals scenarios of transition to the synchronous mode. First, consider the case of small Ω when the frequency-locking scenario of synchronization is observed as a result of SN bifurcation. In Fig. 5, phase portraits in different regimes are presented at different values of Ω and f. The corresponding points in the (Ω, f) plane are shown in Fig. 6. Below the both synchronization tongues, there exist two limit cycles and a stable fixed point O, which originates from the stable zero solution of the free-running oscillator [Fig. 5(a)]. This point corresponds to the regenerative amplification mode as noted above in Sec. III A, while the stable cycle corresponds to the beating mode. The unstable cycle separates the basins of two attractors.

When Ω decreases, the SN bifurcation occurs, which means the birth of the saddle S_1 and the unstable node N_1 on the unstable limit cycle [Fig. 5(b)]. With further decrease in Ω, the second SN bifurcation takes place. Now, the saddle S_2 and the stable node N_2 appear on the stable limit cycle [Fig. 5(c)]. The stable point N_2 corresponds to the injection-locked mode.

When we increase the driving force and cross the upper bound of the SN bifurcation domain, the saddle S_2 collides the unstable node N_1 [Fig. 5(d)]. This bifurcation results in change of the configuration of the basins of attraction of the fixed points. In Fig. 5(c), the basin of the node N_2 is located above the stable manifolds of the saddle S_1, i.e., the high-amplitude injection-locked state settles if the initial amplitude is large enough. In contrast, in Fig. 5(d), the basin is

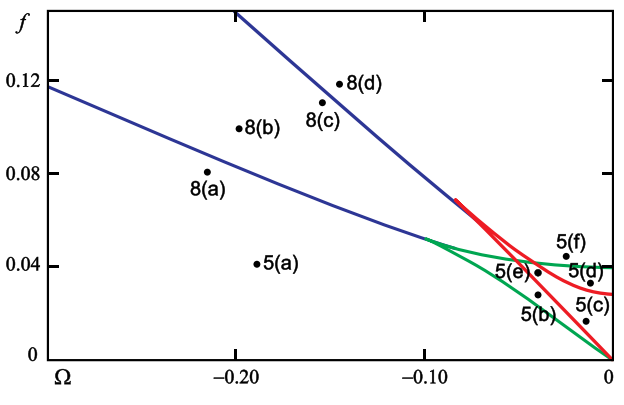

FIG. 6. Enlarged part of the (Ω, f) plane with points at which phase portraits of Figs. 5 and 8 are plotted.

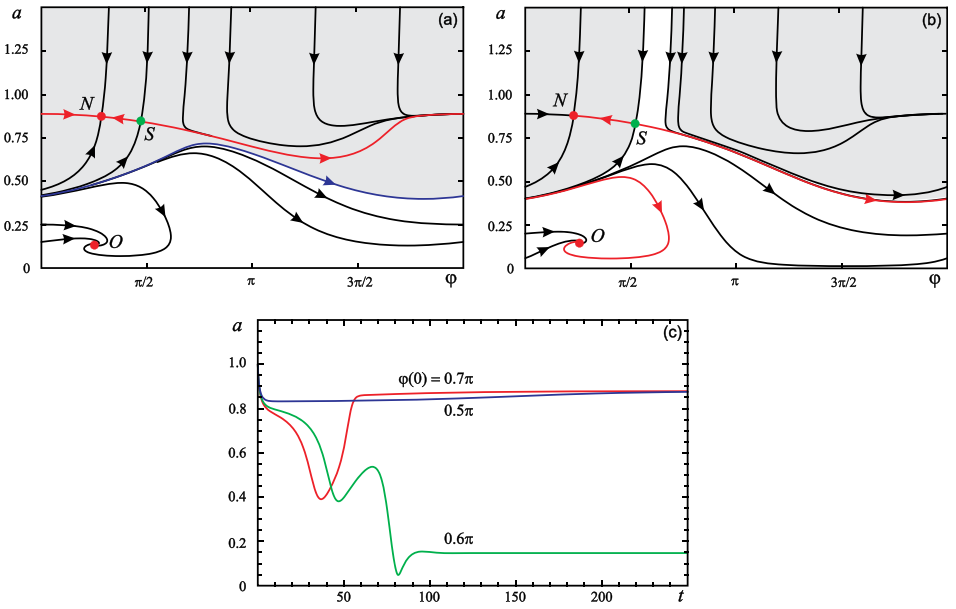

FIG. 7. Phase portraits illustrating the global bifurcation of the unstable limit cycle: $\sigma = -0.21$, $b = -0.22$, $\Omega = -0.2$, $f = 0.037$ (a), and 0.04 (b). Basins of attraction of the high-amplitude injection-locked state are shaded. (c) Transient processes for $a(0) = 1.0$ and different values of $\varphi(0)$.

bounded by the stable manifold of the saddle S_1. In such a case, there appears the band of initial phases near $\varphi(0) \approx \pi$, where the system proceeds to the low-amplitude state O regardless of the initial amplitude value. The process of injection locking is sensitive to the initial phase, and this sensitivity persists until the second saddle-node bifurcation occurs, i.e., the saddle S_1 collides the low-amplitude stable point O. After that, the bistability vanishes and only one stable point N_2 remains [Fig. 5(f)]. Thus, the frequency-locking scenario for the oscillator with hard excitation has obvious differences from the case of soft excitation.[1–4]

At larger frequency mismatch, a slightly different behavior is observed. The stable manifold of S_1 collides with the unstable manifold of S_2. Now, the unstable manifold of S_2 does not close in the node N_2 but leads in the stable point O instead. The phase portrait for this situation is presented in Fig. 5(e). In the phase plane, it remains five fixed points but the basins of attractions change their configuration in the same way as in the previous case.

When the reactive nonlinearity is significant and the bounds of SN bifurcation merge, the frequency-locking scenario is somewhat different. Let us choose $b = -0.22$. The corresponding resonance curves and synchronization tongues are shown in Fig. 4. If the driving frequency is chosen close enough to the free-running oscillator frequency, the first SN bifurcation occurs at the stable cycle [Fig. 7(a)]. With the increase in f, the unstable cycle collides with the unstable manifold of the saddle. The corresponding phase portrait is presented in Fig. 7(b). This global bifurcation results in the change of the configuration of the basins of attraction similar to the situation described in Fig. 5(e). One of the unstable manifolds of the saddle leads to the low-amplitude stable point O instead of N, and at $0.55\pi < \varphi(0) < 0.68\pi$, all phase trajectories tend to the low-amplitude state. This is confirmed by Fig. 7(c) where transient processes for different values of $\varphi(0)$ are shown.

Another scenario is observed at larger values of Ω. In Fig. 5(a), both cycles encircle the phase cylinder, i.e., the phase exhibits infinite drift. When we approach the bound of AH bifurcation, the unstable limit cycle exhibits transformation shown in Fig. 8(a). Now it lies on the side of the phase cylinder surrounding the fixed point. Such a cycle is named contractible. With either an increase in f or a decrease in Ω, it contracts to the O point, which becomes an unstable focus [Fig. 8(b)]. The stable cycle exhibits the same transformations. First, transition to the contractible cycle occurs, as shown in Fig. 8(c). Now the phase φ does not drift but oscillates in a finite band. Such a behavior is sometimes called "phase trapping." Finally, only one stable point remains, which corresponds to the injection-locked state [Fig. 8(d)]. This is a generalization of the transition to synchronization via suppression of natural oscillation.[1–4] During the suppression scenario, the beating amplitude gradually decreases to zero, while during the frequency locking, the beating period tends to infinity.

C. Regenerative amplification below the threshold of hard excitation

Special attention should be paid to the case when the oscillator operates below the threshold of hard excitation ($\sigma < -1/4$), and no oscillation is possible in the free-running system. However, applying the driving signal gives rise to the oscillation with high output power and efficiency. Similar nonlinearly driven oscillation regimes have been demonstrated for gyrotron forward-wave[23] and backward-wave[24] masers. In Fig. 9(a), the pattern of resonance curves is presented for $\sigma = -0.27$. Similar to Fig. 4(a), in Fig. 9(a) there are two domains of stable single-frequency oscillation. In both domains, the oscillator operates as a regenerative amplifier but the output power in the upper domain is much greater than in the lower one.

In Fig. 9(b), the SN and AH bifurcation bounds on the (Ω, f) plane are presented (cf. Sec. III A). The beating domain is shaded. In this domain, the driving signal leads to excitation of the oscillator natural frequency. Minimal threshold of

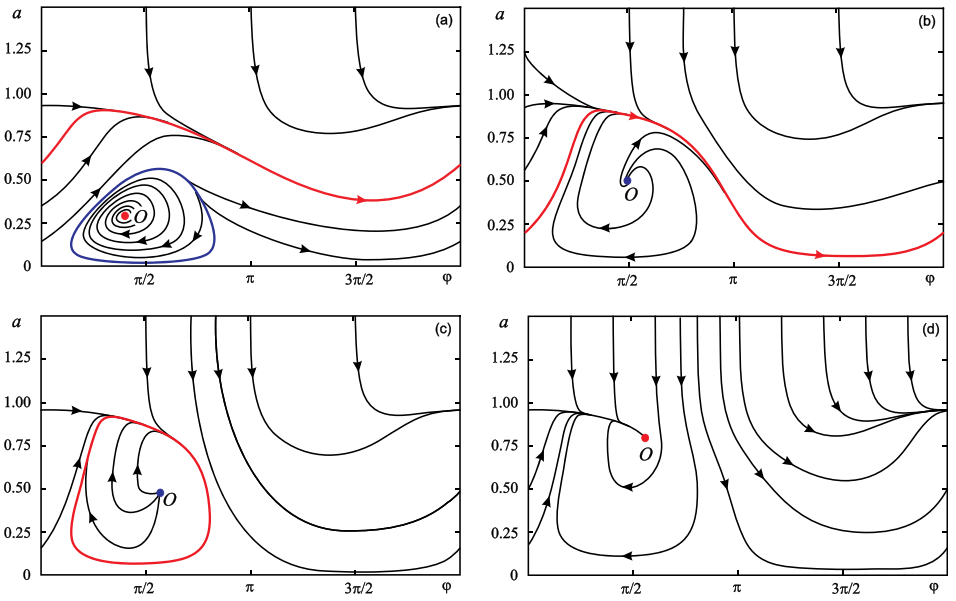

FIG. 8. Phase portraits illustrating the transition to synchronization via the suppression scenario: $\sigma = -0.21$, $b = 0.0$, corresponding values of f and Ω are shown in Fig. 6.

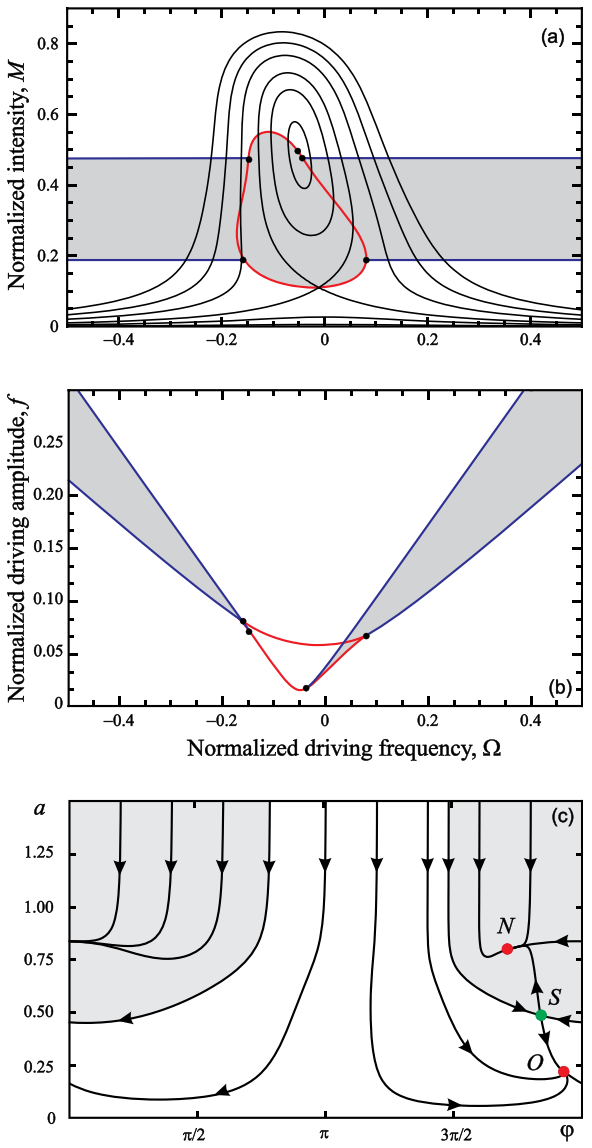

FIG. 9. Resonance curves (a) and stability domains on the (Ω, f) plane (b) for $\sigma = -0.27$, $b = -0.1$; phase portrait for $f = 0.05$, $\Omega = -0.05$ (c). In (c), the basin of attraction of the high-amplitude state N is shaded.

transition to the high-amplitude regime is attained at $f = f_1$, where f_1 is defined by Eq. (11). When we cross the lower SN bound, a saddle S and node N are born on the phase plane. A typical phase portrait is presented in Fig. 9(c). Thus, inside the SN bound both high-amplitude and low-amplitude modes coexist. The basin of attraction of the high-amplitude state has the same structure as in Figs. 5(d) and 7(b). When we cross the upper SN bound, the saddle S collides with the stable point O. After this, only the large-amplitude mode exists.

At $\sigma = -1/3$, the two bounds of the AH bifurcation coincide (see Eq. (12)), and the domains of beating on the (Ω, M) plane vanish. With further decrease in σ, the bound of SN bifurcation shrinks and disappears.

IV. INJECTION LOCKING OF A GYROTRON WITH FIXED GAUSSIAN STRUCTURE OF THE RF FIELD

The quasilinear approximation is valid only at a slight excess of the start-oscillation threshold. In this section, we consider a more adequate time-domain model of a gyrotron with fixed structure of the RF field.[5] In this model, the complex gain factor Φ is obtained from numerical integration of the equations of motion

$$\frac{dp}{d\zeta} + i\left(\Delta + |p|^2 - 1\right)p = iAf_s(\zeta). \tag{13}$$

Here, p is the complex normalized electron orbital momentum, $\Delta = (2/\beta_\perp^2)(1 - \omega_H/\omega_0)$ is the mismatch between the cavity mode eigenfrequency ω_0 and the cyclotron frequency ω_H, $\zeta = (\beta_\perp^2/2\beta_{||})\omega_0 z/c$ is the normalized axial distance, $\beta_\perp = v_\perp/c$, $\beta_{||} = v_{||}/c$, and $f_s(\zeta)$ describes the axial RF-field structure of the cavity mode. For a gyrotron, a Gaussian field profile

$$f_s(\zeta) = \exp\left[-3\left(\frac{2\zeta}{\zeta_k} - 1\right)^2\right], \quad 0 \le \zeta \le \zeta_k$$

often provides a good approximation.[5]

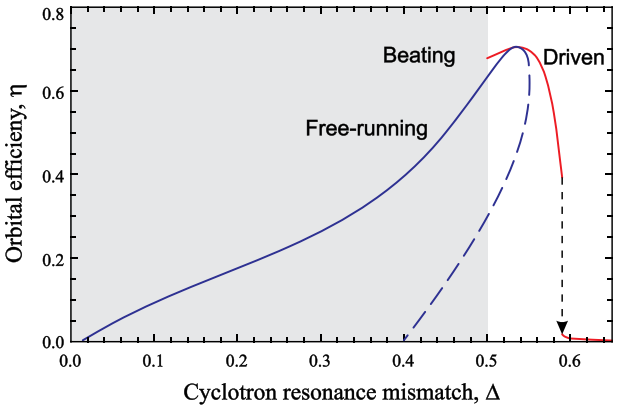

FIG. 10. Orbital efficiency vs. the cyclotron resonance mismatch for the free-running ($f_{inj} = 0$) and driven ($f_{inj} = 0.05$, $\Omega = -0.4\pi$) gyrotron.

From integration of the equations of motion, Eq. (13), with the boundary condition

$$p(\zeta = 0) = \exp(i\varphi_0), \quad \varphi_0 \in [0; 2\pi), \tag{14}$$

one can find the harmonic of the bunched current

$$J = \frac{1}{2\pi}\int_0^{2\pi} p d\varphi_0. \tag{15}$$

Substituting Eq. (15) into the excitation equation, Eq. (1), yields

$$\frac{dA}{d\tau} + A = iI_s \int_0^{\zeta_k} J(\zeta, \tau) f_s^*(\zeta) d\zeta + 2f_{inj} \exp(i\Omega\tau), \tag{16}$$

where $\tau = \omega_0 t/2Q$ is the normalized time.

The electron orbital efficiency is

$$\eta = 1 - \frac{1}{2\pi}\int_0^{2\pi} |p(\zeta_k)|^2 d\varphi_0.$$

Maximal efficiency $\eta \approx 0.7$ is attained at $I_s = 0.06$, $\Delta = 0.53$, and $\mu = 15$, where $\mu = \zeta_k/\sqrt{3}$ is the normalized cavity length. In Fig. 10, η as function of the cyclotron resonance mismatch is plotted. Stable and unstable parts of the curve are shown by solid and dashed lines, respectively. From this figure, one can see that maximal efficiency is attained in the hard excitation mode.

We studied injection-locked operation of a gyrotron with the above-mentioned parameters. In Fig. 11(a), the phase diagram on the driving frequency–driving amplitude parameter plane is presented. The pattern of the phase diagram is qualitatively similar to the quasilinear model studied in Sec. III [cf. Fig. 2(b)]. Above line 1, the domain of injection locking of the gyrotron self-oscillation is located. Maximal efficiency of the phase-locked mode is close to that of the free-running gyrotron, $\eta \approx 0.7$ [Fig. 11(b)]. With the increase in the injection power, the efficiency decreases gradually. When the driving signal amplitude is small enough, the gyrotron operates as a regenerative amplifier. The domain of stable amplification is located below line 2 in Fig. 11(a). In this regime, the efficiency is small, $\eta < 0.1$. In the area where the phase-locking and regenerative amplification domains overlap, i.e., below line 1 but above line 2, there coexist two stable single frequency regimes. In this domain, the oscillator exhibits hysteresis, as shown in Fig. 11(b).

In Fig. 10, the orbital efficiency vs. cyclotron resonance mismatch for a driven gyrotron with $f_{inj} = 0.05$, $\Omega = -0.4\pi$ is presented. For these parameters, at $\Delta = 0.53$, efficiency is the same as for the free-running gyrotron. The driving allows pulling in the domain $\Delta > 0.55$ where there is no free-running oscillation, i.e., the regime of high-power regenerative amplification discussed in Sec. III C is observed. However, the efficiency rapidly decreases with Δ, and at $\Delta \approx 0.6$, a switch to the low-amplitude state occurs. On the other hand, at $\Delta \approx 0.5$ transition to the beating mode occurs.

Fig. 12 illustrates the effect of injection amplitude and frequency on the interaction efficiency. Fig. 12(a) corresponds to $\Delta = 0.53$, i.e., to the regime of maximal efficiency of the free-running gyrotron. The injection-locking bandwidth increases with f_{inj} that is in agreement with Fig. 11(a). Maximal efficiency for the locked gyrotron is nearly the same as for the free-running one, $\eta \approx 0.7$. The maximum shifts towards lower frequencies with the increase in f_{inj}.

The shape of the resonance curves in Fig. 12(a) differs from that of the quasilinear model [Figs. 2(a) and 3(a)]. At the right edge of the locking band, the efficiency grows up to approximately the same values as at the main peak. In such a regime, a validity of the Gaussian fixed-field approximation needs further justification. However, the same shape of $\eta(\Omega)$ curves was reported in Ref. 25 where the injection locking was simulated using the non-fixed field theory.

In the regenerative amplification mode ($\Delta > 0.55$), the resonance curves have similar shape, as shown in Fig. 12(b). The maximal value of η is about 0.635 for $\Delta = 0.57$ and rapidly decreases with Δ.

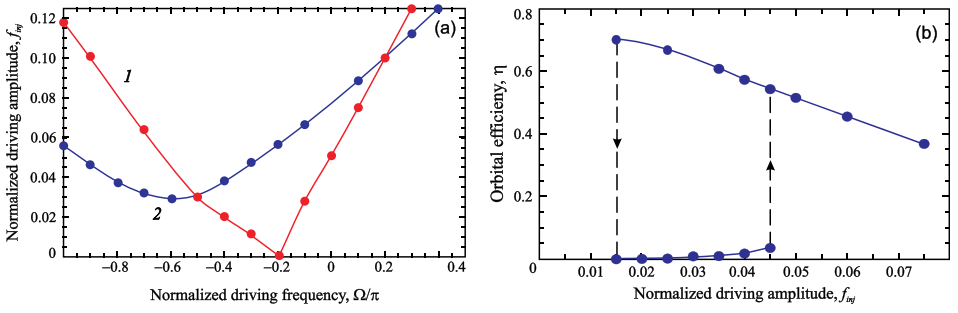

FIG. 11. (a) Bounds of injection locking (1) and regenerative amplification (2) on the (Ω, f_{inj}) plane for $I_s = 0.06$, $\Delta = 0.53$, and $\mu = 15$. (b) Efficiency vs. normalized injection amplitude at $\Omega = -0.3\pi$.

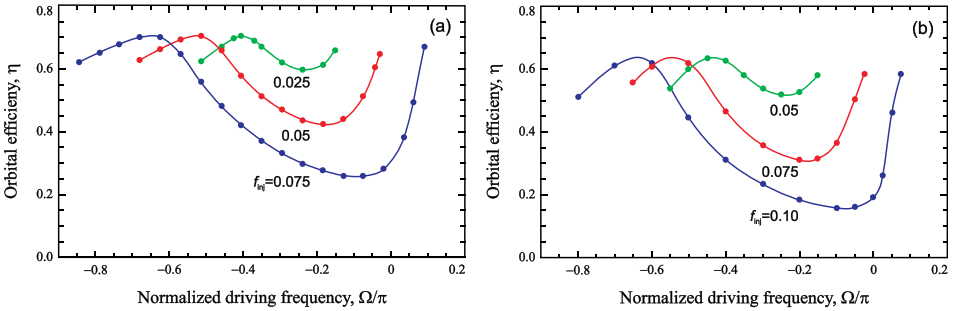

FIG. 12. Orbital efficiency vs. the normalized injection frequency for different values of the injection amplitude for $I_s = 0.06$, $\mu = 15$, $\Delta = 0.53$ (a), and $\Delta = 0.57$ (b).

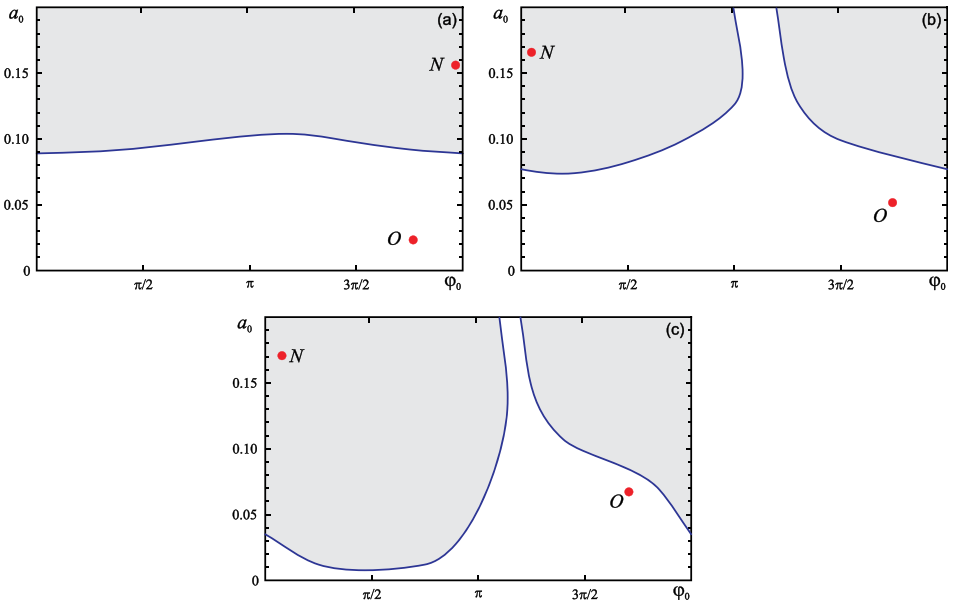

FIG. 13. Basins of attraction of the high-amplitude (N) and low-amplitude (O) steady states for $\Omega = -0.2\pi$, $f_{inj} = 0.015$ (a), 0.035 (b), and 0.0475 (c).

Similar to the quasilinear model (Sec. III B), the injection-locking process may be very sensitive to the initial phase. In Fig. 13, basins of attraction of the high-amplitude and low amplitude steady states are presented for $\Omega = -0.2\pi$, which corresponds to the apex of the synchronization tongue in Fig. 11(a). In this simulation, we integrated the gyrotron equations (13)–(16) with different initial conditions for the cavity field, $A(0) = a_0 \exp(i\varphi_0)$. In Fig. 13(a), the structure of the basins looks similar to Fig. 7(a). In fact, the bound between the two basins is nothing but the unstable limit cycle. For larger f_{inj}, the basins are shown in Figs. 13(b) and 13(c). They acquire the same structure as in Fig. 7(b), which clearly indicates the presence of the saddle point, despite the fact that we are unable to plot the saddle manifolds directly. For $f_{inj} > 0.05$, the bistability vanishes, and the high-amplitude steady state establishes even for very small a_0.

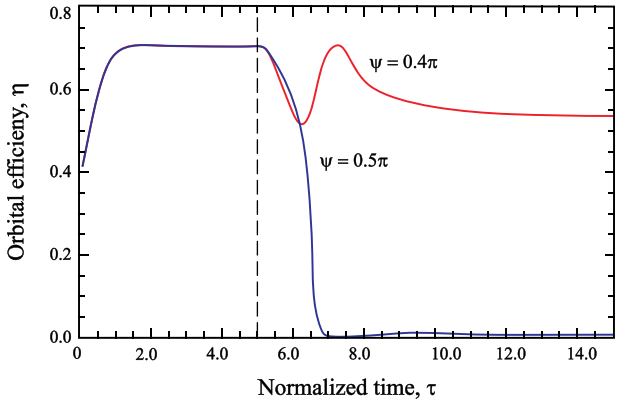

FIG. 14. Orbital efficiency vs. the normalized time for $\Omega = -0.2\pi$, $f_{inj} = 0.035$, and two different values of the initial phase ψ. The moment when the driving signal is switched on is shown with the vertical dashed line.

However, an initial value of amplitude or phase of the cavity field can hardly be controlled experimentally. Therefore, we perform the simulation with more realistic initial conditions, when the driving is injected into the gyrotron oscillator operating in the steady-state free-running mode. In Fig. 14, the corresponding waveforms are presented. The driving signal $f_{inj} \exp(i(\Omega\tau + \psi))$ is switched on at $\tau = 5$, when the steady-state oscillation with $\eta \approx 0.7$ has already been established. Depending on the phase ψ, the driving can either lock the high-efficiency oscillation or switch the gyrotron to the low-efficiency regenerative amplification mode. Thus, the observed transient behavior of the gyrotron is in good agreement with the predictions of the quasilinear model considered in Sec. III.

For better understanding of the results presented in this section, it is important to estimate the power of the injected signal P_{inj}. This power can be obtained from the formula[12,26,27]

$$f_{inj}^2 = \frac{I_s Q}{Q_{cpl}} \frac{P_{inj}}{P_{0\perp}},$$

where Q_{cpl} is the coupling or external Q-factor and $P_{0\perp}$ is the beam power associated with the electron gyration. If we neglect the Ohmic losses, the free-running gyrotron power is $P_f \sim \eta_f P_{0\perp}$, where $\eta_f \approx 0.7$. Assuming that the driver is critically coupled to the cavity one can easily estimate P_{inj}/P_f. For example, three values of f_{inj} in Fig. 13 correspond to $P_{inj}/P_f \sim 0.5\%$, 2.9%, and 5.7%, respectively. Thus, in a typical situation, a rather small driving power is required for the injection locking.

V. CONCLUSION

In this paper, injection locking of an electronic maser in the hard excitation mode is studied. Bifurcation analysis of the quasilinear model (4) described by two ODEs for slowly varying amplitude and phase is presented. Such a model describes a wide class of resonant electronic masers[16–21] operating in a weakly nonlinear regime. The theoretical results are confirmed by numerical simulations of the gyrotron with fixed Gaussian structure of the RF field.

We found several essential differences from the well-known synchronization pattern of an oscillator with soft self-excitation.[1–4] There exist two different modes of single-frequency operation. Depending on the history of the parameter values, the oscillator can operate either as a regenerative amplifier of the input signal or as an injection-locked self-oscillator. With the smooth variation of the injection power, hard transitions between these two modes occur. Depending on the increase or decrease in the injection power, these transitions occur at different values of f_{inj}, i.e., oscillation hysteresis is observed. The low-amplitude regenerative amplification mode is stable if the injection power is low enough. The high-amplitude mode of injection locking is stable inside the tongue-shaped domain, which is similar to a usual synchronization tongue. In the bistability domain, the initial value of the amplitude should be taken large enough to achieve the high-amplitude mode. Moreover, in a certain range of f_{inj}, there is a very sensitive dependence on the initial value of the phase.

Below the hard-excitation threshold, when no self-oscillation in the free-running oscillator is possible, there appear regimes of regenerative amplification with output power and efficiency almost as high as in the free-running oscillator.

ACKNOWLEDGMENTS

This work is supported by the Russian Foundation for Basic Research Grant No. 15-02-02893a.

[1]M. I. Rabinovich and D. I. Trubetskov, *Oscillations and Waves in Linear and Nonlinear Systems* (Kluwer, Dordrecht, 1996).
[2]P. S. Landa, *Regular and Chaotic Oscillations* (Springer, Berlin, 2001).
[3]A. P. Kuznetsov, S. P. Kuznetsov, and N. M. Ryskin, *Nonlinear Oscillations* (Fizmatlit, Moscow, 2005).
[4]V. Anishchenko, V. Astakhov, A. Neiman, T. Vadivasova, and L. Schimansky-Geier, *Nonlinear Dynamics of Chaotic and Stochastic Systems. Tutorial and Modern Developments* (Springer, Berlin, 2007).
[5]G. S. Nusinovich, *Introduction to the Physics of Gyrotrons* (Johns Hopkins University Press, Baltimore, 2004).
[6]V. L. Bakunin, G. G. Denisov, and Y. V. Novozhilova, "Frequency and phase stabilization of a multimode gyrotron with megawatt power by an external signal," Tech. Phys. Lett. **40**, 382–385 (2014).
[7]X. Bai, J. Zhang, J. Yang, and Zh. Jin, "Phase locking of an S-band wide-gap klystron amplifier with high power injection driven by a relativistic backward wave oscillator," Phys. Plasmas **19**, 123103 (2012).
[8]R. Z. Xiao, Z. M. Song, Y. Q. Deng, and C. H. Chen, "Mechanism of phase control in a klystron-like relativistic backward wave oscillator by an input signal," Phys. Plasmas **21**, 093108 (2014).
[9]R. Z. Xiao, C. H. Chen, W. Song, X. W. Zhang, J. Sun, Z. M. Song, L. J. Zhang, and L. G. Zhang, "RF phase control in a high-power high-efficiency klystron-like relativistic backward wave oscillator," J. Appl. Phys. **110**, 013301 (2011).
[10]É. B. Abubakirov, A. N. Denisenko, A. P. Konyushkov, E. I. Soluyanov, and V. V. Yastrebov, "Peculiarities of operation of a relativistic backward-wave oscillator driven by an external electromagnetic signal," Radiophys. Quantum Electron. **57**, 372 (2014).
[11]W. Song, Y. Teng, Z. Q. Zhang, J. W. Li, J. Sun, C. H. Chen, and L. J. Zhang, "Rapid startup in relativistic backward wave oscillator by injecting external backward signal," Phys. Plasmas **19**, 083105 (2012).
[12]G. S. Nusinovich, O. V. Sinitsyn, and T. M. Antonsen, "Mode switching in a gyrotron with azimuthally corrugated resonator," Phys. Rev. Lett. **98**, 205101 (2007).
[13]M. Liu, C. Michel, S. Prasad, M. I. Fuks, E. Schamiloglu, and C.-L. Liu, "RF mode switching in a relativistic magnetron with diffraction output," Appl. Phys. Lett. **97**, 251501 (2010).
[14]M. Liu, C.-L. Liu, D. Galbreath, C. Michel, S. Prasad, M. I. Fuks, and E. Schamiloglu, "Frequency switching in a relativistic magnetron with diffraction output," J. Appl. Phys. **110**, 033304 (2011).
[15]E. N. Starodubova, S. A. Usacheva, N. M. Ryskin, Y. V. Novozhilova, and G. S. Nusinovich, "Injection locking of a two-mode electron oscillator with close frequencies," Phys. Plasmas **22**, 033108 (2015).
[16]G. S. Nusinovich, "Mode interaction in gyrodevices," Int. J. Electron. **51**, 457–474 (1981).
[17]G. S. Nusinovich, L. S. Rodygina, and T. M. Tarantovich, "Theory of synchronization of multimode oscillators with hard self-excitation," Radio Eng. Electron. Phys. **23**, 66–70 (1978).
[18]M. M. Chumakova, S. A. Usacheva, M. Y. Glyavin, Y. V. Novozhilova, and N. M. Ryskin, "Mode competition in a two-mode gyrotron with delayed reflections," IEEE Trans. Plasma Sci. **42**, 2030–2036 (2014).
[19]L. A. Vainshtein, "General theory of resonant electron autooscillators," in *High Power Electronics*, edited by P. L. Kapitza and L. A. Vainshtein (Nauka, Moscow, Russia, 1969), pp. 84–129 (in Russian).
[20]D. I. Trubetskov and A. P. Chetverikov, "Theory of a transition process of a traveling wave in a high-Q relativistic monotron," Radiophys. Quantum Electron. **23**, 159–165 (1980).
[21]W. E. Lamb, Jr., "Theory of an optical maser," Phys. Rev. **134**, A1429 (1964).
[22]A. P. Kuznetsov and S. V. Milovanov, "Synchronization of a self-oscillatory system with bifurcation of merging of a stable and unstable limit cycles," Appl. Nonlinear Dyn. **11**(4–5), 16 (2003) (in Russian).
[23]C. C. Chiu, K. F. Pao, Y. C. Yan, K. R. Chu, L. R. Barnett, and N. C. Luhmann, "Nonlinearly driven oscillations in the gyrotron traveling-wave amplifier," Phys. Plasmas **15**, 123109 (2008).
[24]Y. S. Yeh, T. H. Chang, C. T. Fan, C. L. Hung, J. N. Jhou, J. M. Huang, J. L. Shiao, Z. Q. Wu, and C. C. Chiu, "Nonlinear oscillation behavior of a driven gyrotron backward-wave oscillator," Phys. Plasmas **17**, 113112 (2010).
[25]N. S. Ginzburg, A. S. Sergeev, and I. V. Zotova, "Time-domain self-consistent theory of frequency-locking regimes in gyrotrons with low-Q resonators," Phys. Plasmas **22**, 033101 (2015).
[26]V. S. Ergakov and M. A. Moiseev, "Theory of synchronization of oscillations in a cyclotron-resonance maser monotron by an external signal," Radiophys. Quantum Electron. **18**, 89 (1975).
[27]G. S. Nusinovich, B. G. Danly, and B. Levush, "Gain and bandwidth in stagger-tuned gyroklystrons," Phys. Plasmas **4**, 469 (1997).